

# HOFAR: High-Order Augmentation of Flow Autoregressive Transformers

Yingyu Liang\*    Zhizhou Sha†    Zhenmei Shi‡    Zhao Song§    Mingda Wan¶

## Abstract

Flow Matching and Transformer architectures have demonstrated remarkable performance in image generation tasks, with recent work FlowAR [Ren et al., 2024] synergistically integrating both paradigms to advance synthesis fidelity. However, current FlowAR implementations remain constrained by first-order trajectory modeling during the generation process. This paper introduces a novel framework that systematically enhances flow autoregressive transformers through high-order supervision. We provide theoretical analysis and empirical evaluation showing that our High-Order FlowAR (HOFAR) demonstrates measurable improvements in generation quality compared to baseline models. The proposed approach advances the understanding of flow-based autoregressive modeling by introducing a systematic framework for analyzing trajectory dynamics through high-order expansion.

arXiv:2503.08032v1 [cs.CV] 11 Mar 2025

---

\* yingyu@hku.hk. The University of Hong Kong.    yliang@cs.wisc.edu. University of Wisconsin-Madison.

† shazz20@mails.tsinghua.edu.cn. Tsinghua University.

‡ zhmeishi@cs.wisc.edu. University of Wisconsin-Madison.

§ magic.linuxkde@gmail.com. The Simons Institute for the Theory of Computing at UC Berkeley.

¶ dylan.r.mathison@gmail.com. Anhui University.

# Contents

<b>1</b>	<b>Introduction</b>	<b>2</b>
<b>2</b>	<b>Related Works</b>	<b>2</b>
2.1	Flow-based and Diffusion-based Generative Models . . . . .	2
2.2	High-Order Dynamic Supervision . . . . .	3
<b>3</b>	<b>Preliminary</b>	<b>3</b>
3.1	Notations . . . . .	3
3.2	FlowAR Preprocessing Process . . . . .	4
3.3	Autoregressive Transformer Architecture . . . . .	5
3.4	Flow Matching Architecture . . . . .	7
<b>4</b>	<b>Main Results</b>	<b>9</b>
<b>5</b>	<b>Technical Overview</b>	<b>9</b>
<b>6</b>	<b>Experiments</b>	<b>12</b>
6.1	Experiment Setup . . . . .	13
6.2	Loss Function Curve . . . . .	14
6.3	Visualization Comparison . . . . .	14
<b>7</b>	<b>Conclusion</b>	<b>15</b>
<b>A</b>	<b>Discussion</b>	<b>20</b>
<b>B</b>	<b>Empirical Result</b>	<b>20</b>
B.1	Visualization Examples . . . . .	20

# 1 Introduction

Recently, flow-matching [LCBH<sup>+</sup>22] and diffusion models [HJA20] have demonstrated remarkable capabilities in the field of image generation [RBL<sup>+</sup>22, EKB<sup>+</sup>24]. Several works have explored extending these models to generate images with an additional dimension, such as incorporating a temporal dimension for video generation [SPH<sup>+</sup>22, LCW<sup>+</sup>23] or a 3D spatial dimension for 3D object generation [XXMPM24, Mo24]. Even 4D generation [ZCW<sup>+</sup>25, LYX<sup>+</sup>24] has become feasible using diffusion models. Another prominent line of research focuses on auto-regressive models, where the Transformer framework has achieved groundbreaking success in natural language processing. Models such as GPT-4 [AAA<sup>+</sup>23], Gemini 2 [Dee24], and DeepSeek [GYZ<sup>+</sup>25] have significantly impacted millions of users worldwide.

Given the success of the auto-regressive generation paradigm and the Transformer framework, recent works have explored integrating auto-regressive generation into image generation. A representative example is the Visual Auto-Regressive (VAR) model [TJY<sup>+</sup>25], which introduces hierarchical image generation with different image patches. Other works, such as FlowAR [RYH<sup>+</sup>24] and ARFlow [HZY<sup>+</sup>25], integrate flow-matching with auto-regressive generation. However, these existing approaches primarily focus on modeling the direct transition path between the prior distribution and the target image distribution, paying less attention to high-order dynamics. High-order dynamics play a crucial role in capturing complex dependencies between different modalities, which is especially important for tasks like video generation that require long-term coherence. Moreover, high-order supervision enhances a model’s generalization ability by encouraging it to learn fundamental generative principles rather than relying on lower-order patterns.

Motivated by these insights, we propose High-Order FlowAR (**HOFAR**), an approach that builds upon the strengths of auto-regressive models and flow-matching techniques while extending them to model higher-order interactions. By explicitly incorporating high-order dynamics, HOFAR improves realism, coherence, and generalization in generative tasks. We theoretically prove that HOFAR maintains computational efficiency compared to its base models while empirically demonstrating its superior performance.

In summary, our contributions are as follows:

- We introduce HOFAR, a novel framework that integrates high-order dynamics into flow-matching-based auto-regressive generation, enhancing the model’s ability to capture complex dependencies.
- We provide a theoretical analysis showing that HOFAR maintains computational efficiency while benefiting from high-order modeling.
- We conduct empirical evaluations demonstrating that HOFAR achieves improved generation quality, coherence, and generalization compared to existing auto-regressive generative models.

## 2 Related Works

### 2.1 Flow-based and Diffusion-based Generative Models

Flow-based and diffusion-based generative models have demonstrated significant potential in image and video generation tasks [HJA20, HHS23, LTL<sup>+</sup>24, GXX<sup>+</sup>24, JWT<sup>+</sup>24, XZL<sup>+</sup>24, LZW<sup>+</sup>24]. Among these, Latent Diffusion Models (LDM) [RBL<sup>+</sup>22] have emerged as a particularly powerful approach, especially in the domain of text-to-image synthesis. Recent advancements, such as Stable Diffusion V3 [EKB<sup>+</sup>24], have integrated flow-matching techniques as an alternative strategy to

further improve generation quality and enhance the photorealism of synthesized images. Moreover, a growing body of research [JSL<sup>+</sup>24, WSD<sup>+</sup>24, WCZ<sup>+</sup>23, WXZ<sup>+</sup>24] has highlighted the potential of combining the strengths of diffusion models and flow-matching models to achieve even greater generation fidelity. In this context, we acknowledge several influential works in flow-matching and diffusion-based generation [HST<sup>+</sup>22, SWYY25, DY24, HSZ<sup>+</sup>24, WFQ<sup>+</sup>24, CCL<sup>+</sup>25, LSS<sup>+</sup>25, SSZ<sup>+</sup>24, LLSS24, HWL<sup>+</sup>25, CLL<sup>+</sup>25, KLS<sup>+</sup>25, CGL<sup>+</sup>25a, KLL<sup>+</sup>25, LSSS24, LSS<sup>+</sup>24, GKL<sup>+</sup>25], which have greatly inspired our research.

## 2.2 High-Order Dynamic Supervision

High-order dynamics are often overlooked in the research community, despite their critical role in modeling target distributions—such as image or video distributions—with greater accuracy and effectiveness. Current research primarily explores high-order dynamics within gradient-based methods. For example, solvers [DNG<sup>+</sup>22, HLJ<sup>+</sup>24] and regularization frameworks [KBJD20, FJNO20] for neural ordinary differential equations (neural ODEs) [CRBD18, GCB<sup>+</sup>18] frequently leverage higher-order derivatives to enhance performance [RCK<sup>+</sup>24, CGL<sup>+</sup>25c, CGL<sup>+</sup>25b]. Beyond machine learning, the study of higher-order temporal Taylor methods (TTMs) has been extensively applied to solving both stiff [CC94] and non-stiff [CC94, CC82] systems, demonstrating their broad utility in computational mathematics.

**Roadmap.** This paper is organized as follows: Section 3 introduces the fundamental notations used throughout the paper and provides formal definitions for each module in the proposed model. In Section 4, we present the training and inference algorithms for our HOFAR model, along with an analysis of its computational efficiency. In Section 5, we delve into the technical details and methodologies employed to prove our formal theorem. In Section 6, we conduct an empirical evaluation of the HOFAR model, showcasing its effectiveness and robustness in image generation tasks. Finally, in Section 7, we summarize the key contributions of this paper and provide concluding remarks.

## 3 Preliminary

In this section, we introduce the formal mathematical definitions for the FlowAR model and our High-Order FlowAR (HOFAR) model. These definitions provide the foundational framework for understanding the preprocessing, downsampling, upsampling, and transformer-based components of the proposed architecture. In Section 3.1, we introduce the notations we used in this work. In Section 3.2, we describe the preprocessing steps applied to input images before they are fed into the model. In Section 3.3, we detail the autoregressive Transformer architecture, which generates the conditional embeddings utilized by the flow-matching components in the FlowAR model. Finally, in Section 3.4, we provide a formal mathematical definition of flow modeling and present the implementation of the flow-matching architecture.

### 3.1 Notations

Given a matrix  $X \in \mathbb{R}^{hw \times d}$ , we denote its tensorized form as  $\mathsf{X} \in \mathbb{R}^{h \times w \times d}$ . Additionally, we define the set  $[n]$  to represent  $\{1, 2, \dots, n\}$  for any positive integer  $n$ . We define the set of natural numbers as  $\mathbb{N} := \{0, 1, 2, \dots\}$ . Let  $X \in \mathbb{R}^{m \times n}$  be a matrix, where  $X_{i,j}$  refers to the element at the  $i$ -th row and  $j$ -th column. When  $x_i$  belongs to  $\{0, 1\}^*$ , it signifies a binary number with arbitrary length. In a general setting,  $x_i$  represents a length  $p$  binary string, with each bit taking a value of either

1 or 0. Given a matrix  $X \in \mathbb{R}^{n \times d}$ , we define  $\|X\|_\infty$  as the maximum norm of  $X$ . Specifically,  $\|X\|_\infty = \max_{i,j} |X_{i,j}|$ .

### 3.2 FlowAR Preprocessing Process

We begin by introducing the preprocessing procedure of the FlowAR model. The image is first passed through a Variational Autoencoder (VAE) to obtain a latent image embedding before being processed by the main body of the FlowAR model.

Let  $\mathbf{X} \in \mathbb{R}^{h \times w \times c}$  denote the image embedding generated by the VAE, where  $h$ ,  $w$ , and  $c$  represent the height, width, and number of channels, respectively. The next step involves downsampling the image embedding  $\mathbf{X}$  to multiple scales. To formalize this process, we first define the linear downsampling function.

**Definition 3.1** (Linear Downsampling Function). *If the following conditions hold:*

- Let  $\mathbf{X} \in \mathbb{R}^{h \times w \times c}$  denote the input tensor, where  $h, w, c$  represent height, width, and the number of channels, respectively.
- Let the positive integer  $r \geq 1$  denote the scaling factor.

The linear downsampling function  $\phi_{\text{down}}(\mathbf{X}, r)$  computes an output tensor  $\mathbf{Y} \in \mathbb{R}^{(h/r) \times (w/r) \times c}$ .

To be more specific, let  $\Phi_{\text{down}} \in \mathbb{R}^{(h/r \cdot w/r) \times hw}$  denote a linear transformation matrix. The downsampling transformation consists of three steps:

- Reshape  $\mathbf{X}$  into the matrix  $X \in \mathbb{R}^{hw \times c}$  by flattening its spatial dimensions.
- Apply the linear transformation matrix  $\Phi_{\text{down}}$  on  $X$  as

$$Y = \Phi_{\text{down}} X \in \mathbb{R}^{(h/r \cdot w/r) \times c},$$

- Reshaped back to  $\mathbf{Y} \in \mathbb{R}^{(h/r) \times (w/r) \times c}$ .

Next, we define the multi-scale downsampling tokenizer, which leverages the linear downsampling function to generate a sequence of token maps at multiple scales.

**Definition 3.2** (Multi-Scale Downsampling Tokenizer). *If the following conditions hold:*

- Let  $\mathbf{X} \in \mathbb{R}^{h \times w \times c}$  denote the image embedding generated by VAE.
- Let  $K \in \mathbb{N}$  denote the number of scales.
- Let the positive integer  $a \geq 1$  denote the base scaling factor.
- For  $i \in [K]$ , we define scale-specific factors  $r_i := a^{K-i}$  and use the linear downsampling function  $\phi_{\text{down}}(\mathbf{X}, r_i)$  from Definition 3.1.

We define the multi-scale downsampling tokenizer as  $\text{TN}(\mathbf{X}) := \{\mathbf{Y}^1, \dots, \mathbf{Y}^K\}$ , which outputs a sequence of token maps  $\{\mathbf{Y}^1, \mathbf{Y}^2, \dots, \mathbf{Y}^K\}$ , where the  $i$ -th token map is generated by

$$\mathbf{Y}^i := \phi_{\text{down},i}(\mathbf{X}, r_i) \in \mathbb{R}^{(h/r_i) \times (w/r_i) \times c},$$

During inference, we need to upsample the embeddings after each processing step. To formalize this operation, we define the bicubic upsampling function as follows.

**Definition 3.3** (Upsampling Function). *If the following conditions hold:*

- Let  $\mathbf{X} \in \mathbb{R}^{h \times w \times c}$  denote the input tensor, where  $h, w, c$  represent height, width, and the number of channels, respectively.
- Let the  $A$  positive integer  $r \geq 1$  denote the scaling factor.
- Let  $W : \mathbb{R} \rightarrow [0, 1]$  denote the bicubic kernel.

We define the bicubic upsampling function as  $\phi_{\text{up}}(\mathbf{X}, r)$ , which computes  $\mathbf{Y} \in \mathbb{R}^{rh \times rw \times c}$ . For every output position  $i \in [rh], j \in [rw], l \in [c]$ :

$$Y_{i,j,l} = \sum_{s=-1}^2 \sum_{t=-1}^2 W(s) \cdot W(t) \cdot X_{\lfloor \frac{i}{r} \rfloor + s, \lfloor \frac{j}{r} \rfloor + t, l}$$

### 3.3 Autoregressive Transformer Architecture

The downsampled embeddings are then fed into the transformer architecture to generate the condition tensor for the flow matching model. The autoregressive transformer is a key component of the FlowAR model. Below, we define its attention layer, feedforward layer, and the overall autoregressive transformer.

**Definition 3.4** (Attention Layer). *If the following conditions hold:*

- Let  $\mathbf{X} \in \mathbb{R}^{h \times w \times c}$  denote the input tensor, where  $h, w, c$  represent height, width, and the number of channels, respectively.
- Let  $W_Q, W_K, W_V \in \mathbb{R}^{c \times c}$  denote the weight matrices, which will be used in query, key, and value projection, respectively.

The attention layer  $\text{Attn}(\mathbf{X})$  is defined by computing the output tensor  $\mathbf{Y} \in \mathbb{R}^{h \times w \times c}$  in the following three steps:

- Reshape  $\mathbf{X}$  into a matrix  $X \in \mathbb{R}^{hw \times c}$  with spatial dimensions collapsed.
- Attention matrix computation. For  $i, j \in [hw]$ , compute pairwise scores:

$$A_{i,j} := \exp(X_{i,*} W_Q W_K^T X_{j,*}^T), \text{ for } i, j \in [hw].$$

- Normalization. Compute diagonal matrix  $D := \text{diag}(A \mathbf{1}_n) \in \mathbb{R}^{hw \times hw}$ , where  $\mathbf{1}_n$  is the all-ones vector. And compute:

$$Y := D^{-1} A X W_V \in \mathbb{R}^{hw \times c}.$$

- Reshape  $Y$  to  $\mathbf{Y} \in \mathbb{R}^{h \times w \times c}$ .

The feedforward layer is another critical component of the transformer architecture. We define it as follows.

**Definition 3.5** (Feed Forward Layer). *If the following conditions hold:*

- Let  $\mathbf{X} \in \mathbb{R}^{h \times w \times c}$  denote the input tensor, where  $h, w, c$  represent height, width, and the number of channels, respectively.

- Let  $W_1, W_2 \in \mathbb{R}^{c \times d}$  denote the weight matrices and  $b_1, b_2 \in \mathbb{R}^{1 \times d}$  denote the bias vectors.
- Let  $\sigma : \mathbb{R} \rightarrow \mathbb{R}$  denote the ReLU activation function which is applied element-wise.

We defined the feedforward operation as  $Y := \text{FFN}(X)$ .

To be more specific, it computes an output tensor  $Y \in \mathbb{R}^{h \times w \times c}$  in the following steps:

- Reshape  $X$  into a matrix  $X \in \mathbb{R}^{hw \times c}$  with spatial dimensions collapsed.
- For each  $j \in [hw]$ , compute

$$Y_{j,*} = \underbrace{X_{j,*}}_{1 \times c} + \sigma \left( \underbrace{X_{j,*}}_{1 \times c} \cdot \underbrace{W_1}_{c \times c} + \underbrace{b_1}_{1 \times c} \right) \cdot \underbrace{W_2}_{c \times c} + \underbrace{b_2}_{1 \times c} \in \mathbb{R}^{1 \times c}$$

where  $\sigma$  acts element-wise on intermediate results. Then reshape  $Y \in \mathbb{R}^{hw \times c}$  into  $Y \in \mathbb{R}^{h \times w \times c}$ .

Using the attention and feedforward layers, we now define the autoregressive transformer.

**Definition 3.6** (Autoregressive Transformer). *If the following conditions hold:*

- Let  $X \in \mathbb{R}^{h \times w \times c}$  denote the input tensor, where  $h, w, c$  represent height, width, and the number of channels, respectively.
- Let  $K \in \mathbb{N}$  denote the scale number, which is the number of total scales in FlowAR.
- For  $i \in [K]$ , let  $Y_i \in \mathbb{R}^{(h/r_i) \times (w/r_i) \times c}$  denote the token maps generated by the Multi-Scale downsampling tokenizer defined in Definition 3.2 where  $r_i = a^{K-i}$  with base  $a \in \mathbb{N}^+$ .
- For  $i \in [K]$ , let  $\phi_{\text{up},i}(\cdot, a) : \mathbb{R}^{(h/r_i) \times (w/r_i) \times c} \rightarrow \mathbb{R}^{(h/r_{i+1}) \times (w/r_{i+1}) \times c}$  denote the upsampling functions as defined in Definition 3.3.
- For  $i \in [K]$ , let  $\text{Attn}_i(\cdot) : \mathbb{R}^{(\sum_{j=1}^i h/r_j \cdot w/r_j) \times c} \rightarrow \mathbb{R}^{(\sum_{j=1}^i h/r_j \cdot w/r_j) \times c}$  denote the attention layer which acts on flattened sequences of dimension defined in Definition 3.4.
- For  $i \in [K]$ , let  $\text{FFN}_i(\cdot) : \mathbb{R}^{(\sum_{j=1}^i h/r_j \cdot w/r_j) \times c} \rightarrow \mathbb{R}^{(\sum_{j=1}^i h/r_j \cdot w/r_j) \times c}$  denote the feed forward layer which acts on flattened sequences of dimension defined in Definition 3.5.
- Let  $Z_{\text{init}} \in \mathbb{R}^{(h/r_1) \times (w/r_1) \times c}$  denote the initial condition embedding which encodes class information.

Then, the autoregressive processing is:

- **Initialization:** Let  $Z_1 := Z_{\text{init}}$ .
- **Iterative sequence construction:** For  $i \geq 2$ .

$$Z_i := \text{Concat}(Z_{\text{init}}, \phi_{\text{up},1}(Y^1, a), \dots, \phi_{\text{up},i-1}(Y^{i-1}, a))$$

where  $\text{Concat}$  reshapes tokens into a unified spatial grid.

- **Transformer block:** For  $i \in [K]$ ,

$$\text{TF}_i(Z_i) := \text{FFN}_i(\text{Attn}_i(Z_i)) \in \mathbb{R}^{(\sum_{j=1}^i h/r_j \cdot w/r_j) \times c}$$

- **Output decomposition:** Extract the last scale's dimension from the reshaped  $\text{TF}_i(Z_i)$  to generate  $\hat{Y}_i \in \mathbb{R}^{(h/r_i) \times (w/r_i) \times c}$ .

### 3.4 Flow Matching Architecture

We begin by outlining the concept of velocity flow in the flow-matching architecture. This section introduces the foundational definitions and components necessary to understand the flow-matching model.

**Definition 3.7** (Flow). *If the following conditions hold:*

- Let  $\mathbf{X} \in \mathbb{R}^{h \times w \times c}$  denote the input tensor, where  $h, w, c$  represent height, width, and the number of channels, respectively.
- Let  $K \in \mathbb{N}$  denote the scales number.
- For  $i \in [K]$ , let  $\mathbf{F}_i^0 \in \mathbb{R}^{(h/r_i) \times (w/r_i) \times c}$  denote the noise tensor with every entry sampled from  $\mathcal{N}(0, 1)$ .
- For  $i \in [K]$ , let  $\hat{\mathbf{Y}}_i \in \mathbb{R}^{(h/r_i) \times (w/r_i) \times c}$  denote the token maps generated by autoregressive transformer as defined in Definition 3.6.

Then, we define the flow model supports the following two operations:

- **Interpolation:** For timestep  $t \in [0, 1]$  and scale  $i$ ,

$$\mathbf{F}_i^t := t\hat{\mathbf{Y}}_i + (1-t)\mathbf{F}_i^0$$

which describes a linear trajectory between the noise  $\mathbf{F}_i^0$  and target tokens  $\hat{\mathbf{Y}}_i$ .

- **Velocity Field:** The time derivative of the flow at scale  $i$  is given by

$$\mathbf{V}_i^t := \frac{d\mathbf{F}_i^t}{dt} = \hat{\mathbf{Y}}_i - \mathbf{F}_i^0.$$

This velocity field is constant across  $t$  due to the linear nature of the interpolation.

Before introducing the implementation of the flow-matching model, we first define two essential components: the Multi-Layer Perceptron (MLP) layer and the Layer Normalization (LN) layer. These components are critical for constructing the flow-matching architecture.

**Definition 3.8** (MLP Layer). *If the following conditions hold:*

- Let  $\mathbf{X} \in \mathbb{R}^{h \times w \times c}$  denote the input tensor, where  $h, w, c$  represent height, width, and the number of channels, respectively.
- Let  $\mathbf{W} \in \mathbb{R}^{c \times d}$  denote the weight matrix and  $\mathbf{b} \in \mathbb{R}^{1 \times d}$  denote the bias vector.

We define the MLP layer as  $\mathbf{Y} := \text{MLP}(\mathbf{X}, c, d)$ , which outputs tensor  $\mathbf{Y} \in \mathbb{R}^{h \times w \times d}$  by using the following operations:

- Reshape  $\mathbf{X}$  into a matrix  $X \in \mathbb{R}^{hw \times c}$  with spatial dimensions collapsed.
- For all  $j \in [hw]$ , we apply affine transformation on each row as follows

$$Y_{j,*} = \underbrace{X_{j,*}}_{1 \times c} \cdot \underbrace{\mathbf{W}}_{c \times d} + \underbrace{\mathbf{b}}_{1 \times d}$$

- Reshape  $Y \in \mathbb{R}^{hw \times d}$  into  $Y \in \mathbb{R}^{h \times w \times d}$ .

Next, we define the Layer Normalization layer, which is a key component for stabilizing and normalizing the inputs to the flow-matching architecture.

**Definition 3.9** (Layer Normalization Layer). *If the following conditions hold:*

- Let  $X \in \mathbb{R}^{h \times w \times c}$  denote the input tensor, where  $h, w, c$  represent height, width, and the number of channels, respectively.

We define the layer normalization as  $Y := \text{LN}(X)$ , which computes  $Y$  through the following steps

- Reshape  $X$  into a matrix  $X \in \mathbb{R}^{hw \times c}$  with spatial dimensions collapsed.
- For each  $j \in [hw]$ , we apply normalization on each row of the matrix,

$$Y_{j,*} = (X_{j,*} - \mu_j) \sigma_j^{-1}$$

where

$$\mu_j := \sum_{k=1}^c X_{j,k}/c, \quad \sigma_j = \left( \sum_{k=1}^c (X_{j,k} - \mu_j)^2 / c \right)^{1/2}$$

- Reshape  $Y \in \mathbb{R}^{hw \times c}$  into  $Y \in \mathbb{R}^{h \times w \times c}$ .

With the MLP and Layer Normalization layers defined, we now introduce the flow-matching layer, which is a core component of the FlowAR model.

**Definition 3.10** (Flow Matching Architecture). *If the following conditions hold:*

- Let  $X \in \mathbb{R}^{h \times w \times c}$  denote the input tensor, where  $h, w, c$  represent height, width, and the number of channels, respectively.
- Let  $K \in \mathbb{N}$  denote the number of total scales in FlowAR.
- For  $i \in [K]$ , let  $\hat{Y}_i \in \mathbb{R}^{(h/r_i) \times (w/r_i) \times c}$  denote the token maps generated by autoregressive transformer defined in Definition 3.6.
- For  $i \in [K]$ , let  $F_i^t \in \mathbb{R}^{(h/r_i) \times (w/r_i) \times c}$  denote interpolated input defined in Definition 3.7.
- For  $i \in [K]$ , let  $t_i \in [0, 1]$  denote timestep.
- For  $i \in [K]$ , let  $\text{Attn}_i(\cdot) : \mathbb{R}^{h/r_i \times w/r_i \times c} \rightarrow \mathbb{R}^{h/r_i \times w/r_i \times c}$  denote the attention layer as defined in Definition 3.4.
- For  $i \in [K]$ , let  $\text{MLP}_i(\cdot, c, d) : \mathbb{R}^{h/r_i \times w/r_i \times c} \rightarrow \mathbb{R}^{h/r_i \times w/r_i \times c}$  denote the MLP layer as defined in Definition 3.8.
- For  $i \in [K]$ , let  $\text{LN}_i(\cdot) : \mathbb{R}^{h/r_i \times w/r_i \times c} \rightarrow \mathbb{R}^{h/r_i \times w/r_i \times c}$  denote the layer norm layer as defined in Definition 3.9.

Then we define the flow-matching architecture as  $F_i^{t_i} := \text{FM}_i(\hat{Y}_i, F_i^{t_i}, t_i)$ , which contains the following computation steps:

- Generate parameter conditioned on the timestep,

$$\alpha_1, \alpha_2, \beta_1, \beta_2, \gamma_1, \gamma_2 := \text{MLP}_i(\widehat{Y}_i + t_i, c, 6c)$$

- Apply attention mechanism,

$$F_i^{t_i} := \text{Attn}_i(\gamma_1 \circ \text{LN}(F_i^{t_i}) + \beta_1) \circ \alpha_1$$

with  $\circ$  denoting Hadamard (element-wise) product.

- Apply MLP and LN modules,

$$F_i^{t_i} := \text{MLP}_i(\gamma_2 \circ \text{LN}(F_i^{t_i}) + \beta_2, c, c) \circ \alpha_2$$

## 4 Main Results

In this section, we present our theoretical analysis of the computational efficiency of the HOFAR model. We demonstrate that despite incorporating high-order dynamics supervision, the increase in computational complexity for both training and inference remains marginal compared to the significant performance improvements achieved.

**Theorem 4.1** (Computational Efficiency of HOFAR). *In accordance with Definition 3.6, the auto-regressive Transformer architecture incorporates  $m$  attention layers. The image input  $x_{\text{img}} \in \mathbb{R}^{n \times n \times c}$  is encoded with  $n^2$  spatial units,  $c$  channels, and a  $d$ -dimensional latent representation. The HOFAR model demonstrates computational costs of  $O(kmn^4d^2)$  for both training and inference under the specified structural constraints.*

*Proof.* The proof follows from Lemma 5.3 and Lemma 5.4. □

## 5 Technical Overview

In this section, we present the key lemmas used to prove the main theorem introduced in the previous section. Specifically, we first analyze the computational complexity of each component in auto-regressive Transformers and the Flow-Matching architecture. Then, we integrate these results to derive the overall runtime for both the Transformer and Flow-Matching components.

We begin by analyzing the runtime of the auto-regressive Transformer module.

**Lemma 5.1** (Running time for Auto-Regressive Transformer Forward). *Let the auto-regressive Transformer be defined as in Definition 3.6 and that it contains  $m$  attention layers. Let  $x_{\text{img}} \in \mathbb{R}^{n \times n \times c}$  be the input image, where  $n$  denotes the resolution and  $c$  denotes the number of channels, and let  $d$  denote the hidden dimension. Under these conditions, the running time for a single forward pass of the auto-regressive Transformer is  $O(mn^4d)$ .*

*Proof.* We consider each attention block in the Transformers architecture.

For each attention block, it consists of the following three steps:

**Step 1: Generate matrices  $Q, K, V$ .** We need to generate a query vector  $q \in \mathbb{R}^d$ , a key vector  $k \in \mathbb{R}^d$  and a value vector  $v \in \mathbb{R}^d$  for each pixel in the original  $n \times n$  image  $x_{\text{img}}$ . After this step, we will have three matrices  $Q, K, V \in \mathbb{R}^{n^2 \times d}$ . This step takes  $O(n^2d)$  time.

---

**Algorithm 1** High-Order FlowAR Training

---

```
1: procedure HOFARTRAINING( $\theta, D$ )
2:   /*  $\theta$  denotes the model parameters of TF, FMfirst, FMsecond */
3:   /*  $D$  denotes the training dataset. */
4:   while not converged do
5:     /* Sample an image from dataset. */
6:      $x_{\text{img}} \sim D$ 
7:     /* Init loss as 0. */
8:      $\ell \leftarrow 0$ 
9:     /* Train the model on  $K$  pyramid layers. */
10:    for  $i = 1 \rightarrow K$  do
11:      /* Sample random noise. */
12:       $\mathbf{F}^0 \sim \mathcal{N}(0, I)$ 
13:      /* Sample a random timestep. */
14:       $t \sim [0, 1]$ 
15:      /* Calculate noisy input. */
16:       $\mathbf{F}_{\text{noisy}}^t \leftarrow \alpha_t x_{\text{img}} + \beta_t \mathbf{F}_i^0$ 
17:      /* Calculate first-order ground-truth. */
18:       $\mathbf{F}_{\text{first}}^t \leftarrow \alpha'_t x_{\text{img}} + \beta'_t \mathbf{F}_i^0$ 
19:      /* Calculate second-order ground-truth. */
20:       $\mathbf{F}_{\text{second}}^t \leftarrow \alpha''_t x_{\text{img}} + \beta''_t \mathbf{F}_i^0$ 
21:      /* Generate condition with Transformer. */
22:       $\hat{\mathbf{Y}} \leftarrow \text{TF}(x_{\text{img}})$ 
23:      /* Predict first-order with FM. */
24:       $\hat{\mathbf{F}}_{\text{first}}^t \leftarrow \text{FM}_{\text{first}}(\mathbf{F}_{\text{noisy}}^t, \hat{\mathbf{Y}})$ 
25:      /* Predict second-order with FM. */
26:       $\hat{\mathbf{F}}_{\text{second}}^t \leftarrow \text{FM}_{\text{second}}(\mathbf{F}_{\text{noisy}}^t, \hat{\mathbf{Y}})$ 
27:      /* Calculate loss. */
28:       $\ell_c \leftarrow \|\hat{\mathbf{F}}_{\text{first}}^t - \mathbf{F}_{\text{first}}^t\|_2^2 + \|\hat{\mathbf{F}}_{\text{second}}^t - \mathbf{F}_{\text{second}}^t\|_2^2$ 
29:       $\ell \leftarrow \ell + \ell_c$ 
30:      /* Downsample  $x_{\text{img}}$  for next iteration. */
31:       $x_{\text{img}} \leftarrow \Phi_{\text{down}} x_{\text{img}}$ 
32:    end for
33:    /* Optimize parameter  $\theta$  with  $\ell$ . */
34:     $\theta \leftarrow \nabla_{\theta} \ell$ 
35:  end while
36:  return  $\theta$ 
37: end procedure
```

---

**Step 2: Calculate the attention matrix.** As defined in Definition 3.4, we need to calculate the attention matrix. It takes  $O(n^4d)$  to calculate  $QK^\top \in \mathbb{R}^{n^2 \times n^2}$ . It takes  $O(n^4)$  time to calculate  $\exp(QK^\top)$ . It takes  $O(n^2)$  time to calculate  $D = \exp(QK^\top) \mathbf{1}_{n^2}$ . It takes  $O(n^2)$  to calculate the  $D^{-1}$ . It takes  $O(n^4)$  to multiply  $D^{-1}$  to each row of  $\exp(QK^\top)$ . The overall running time is  $O(n^4d)$ . After this step, we will get the attention matrix  $A \in \mathbb{R}^{n^2 \times n^2}$ .

**Step 3: Calculate the final output.** The final step is to calculate  $A \cdot V$ . Since  $A \in \mathbb{R}^{n^2 \times n^2}$  and  $V \in \mathbb{R}^{n^2 \times d}$ . The running time of this step is  $O(n^4d)$ . Therefore, according to the above analysis, the running time for a single attention operation is  $O(n^4d)$ . Since there are total  $m$

---

**Algorithm 2** High-Order FlowAR Inference

---

```
1: procedure HOFARINFERENCE( $c_{\text{input}}$ )
2:   /*  $c_{\text{input}}$  denotes the condition embedding used for generation. */
3:   /* Init the Transformer input  $x$  with  $c_{\text{input}}$ . */
4:    $x \leftarrow c_{\text{input}}$ 
5:   /* Init the  $x_{\text{img}}$  with random noise. */
6:    $x_{\text{img}} \leftarrow \mathcal{N}(0, I)$ 
7:   /* Inference through  $K$  pyramid scales. */
8:   for  $i = 1 \rightarrow K$  do
9:     /* Pass through the Transformers TF. */
10:     $\hat{Y} \leftarrow \text{TF}(x)$ 
11:    /* Extract last  $i * i$  tokens from  $Y$  as the condition embedding. */
12:     $x_{\text{cond}} \leftarrow Y[\dots, -i * i :]$ 
13:    /* Generate first-order with  $\text{FM}_{\text{first}}$ . */
14:     $\hat{y}_{\text{first}} \leftarrow \text{FM}_{\text{first}}(x_{\text{cond}}, x_{\text{img}})$ 
15:    /* Generate second-order with  $\text{FM}_{\text{second}}$ . */
16:     $\hat{y}_{\text{second}} \leftarrow \text{FM}_{\text{second}}(x_{\text{cond}}, x_{\text{img}})$ 
17:    /* Apply first and second-order terms. */
18:     $x_{\text{img}} \leftarrow x_{\text{img}} + \hat{y}_{\text{first}} \cdot \Delta t + 0.5 \cdot \hat{y}_{\text{second}} \cdot (\Delta t)^2$ 
19:    /* Upsample  $x_{\text{img}}$ . */
20:     $x_{\text{img}} \leftarrow \phi_{\text{up}}(x_{\text{img}})$ 
21:    /* Concatenate upsampled  $x_{\text{img}}$  to the Transformer input. */
22:     $x \leftarrow \text{Concat}(x, x_{\text{img}})$ 
23:  end for
24:  /* Return the final image */
25:  return  $x_{\text{img}}$ 
26: end procedure
```

---

attention layers in the auto-regressive Transformer, the overall running time is  $O(mn^4d)$ .  $\square$

Another crucial component of the HOFAR model is the flow-matching architecture. Following a similar approach, we analyze the computational complexity of the flow-matching model as follows:

**Lemma 5.2** (Running time for Flow-Matching Forward). *Let the auto-regressive Transformer TF be defined as in Definition 3.6 and that the flow-matching architecture is defined as in Definition 3.10. Let  $x_{\text{img}} \in \mathbb{R}^{n \times n \times c}$  denote the image, where  $n$  denotes the resolution and  $c$  denotes the number of channels, and let  $d$  denote the hidden dimension. Under these conditions, we can show that the running time for a single forward pass of the flow-matching architecture is  $O(n^4d^2)$ .*

*Proof.* Since the input of the flow-matching is the output of the auto-regressive Transformer, which is  $\text{TF}(x_{\text{img}}) \in \mathbb{R}^{n^2 \times n^2 \times d}$ . According to the definition of flow-matching architecture (Definition 3.10), it consists of three operations: one MLP layer, one attention layer, and one MLP layer. For the first layer, the MLP layer, the running complexity is  $O(n^2d^2)$ . For the second layer, the attention layer, according to the proof of Lemma 5.1, the running time for this layer is  $O(n^4d)$ . For the third layer, the MLP layer, the running complexity is  $O(n^2d^2)$ . Therefore, the overall running time for the flow-matching is  $O(n^4d^2)$ .  $\square$

With the runtime analysis of both the Transformer and Flow-Matching modules completed, we now proceed to analyze the training procedure of the HOFAR model. In the following proof, we break down the training process step by step and derive the overall computational complexity at the end.

**Lemma 5.3** (Running time for HOFAR training). *Suppose that the auto-regressive Transformer is defined as in Definition 3.6 and contains  $m$  attention layers. Let the flow-matching architecture be defined as in Definition 3.10, and assume that the HOFAR training process is described in Algorithm 1. Furthermore, suppose that HOFAR consists of  $k$  pyramid frames, let  $d$  denote the hidden dimension, and let  $x_{\text{img}} \in \mathbb{R}^{n \times n \times c}$  denote the image with resolution  $n$  and  $c$  channels. Then, the running time of the training procedure of HOFAR is  $O(kmn^4d^2)$ .*

*Proof.* We first consider the running time for each pyramid frame in the training loop (Line 11 to 31 in Algorithm 1). In each loop, we first consider time complexity for the preparation of essential variables (Line 15 to 20). Since the dimension of each variable in this process is  $n \times n \times d$ , the running complexity for the preparation process is  $O(n^2d)$ . Then, we consider the process of generating condition embeddings with Transformer (Line 22). According to Lemma 5.1, the running time for this process is  $O(mn^4d)$ . Next, according to Lemma 5.2, the prediction process of the flow-matching models takes  $O(n^4d^2)$  time. Finally, the loss calculation step (Line 28) takes  $O(n^2d)$  time.

Therefore, according to all the analysis mentioned above, the running time for each iteration is  $O(mn^4d^2)$ .

Since there are total  $k$  pyramid frames, the overall running time for the training process is  $O(kmn^4d^2)$ . □

Following a similar procedure, we can have the running complexity analysis for the inference procedure as follows:

**Lemma 5.4** (Running time for HOFAR inference). *Let the auto-regressive Transformer be defined as in Definition 3.6 and contain  $m$  attention layers, that the flow-matching architecture is defined as in Definition 3.10, and that the HOFAR inference process is described in Algorithm 2. Also, suppose there are  $k$  pyramid frames in HOFAR and let  $d$  denote the hidden dimension. Under these conditions, the running time of the HOFAR inference procedure is  $O(kmn^4d^2)$ .*

*Proof.* We begin with considering each loop in  $k$ -th inference (Line 9 to Line 22). For each loop, according to Lemma 5.1, the Transformer forward pass (Line 10) takes  $O(mn^4d)$  time. Next, according to Lemma 5.2, the flow-matching prediction process (Line 13 - 16) takes  $O(n^4d^2)$  time. Finally, the time for applying the predicted gradient on image (Line 18) takes  $O(n^2d)$  time. Therefore, the overall running time for each inference loop is  $O(mn^4d^2)$ . Since there are total  $k$  inference loops, the overall running time is  $O(kmn^4d^2)$ . □

Combining all the analyses discussed above, we can directly arrive at our final theorem (Theorem 4.1).

## 6 Experiments

In Section 6.1, we introduce the setting we used in our experiments. In Section 6.2, we present the loss curve of the various models. In Section 6.3, we present visualization examples produced

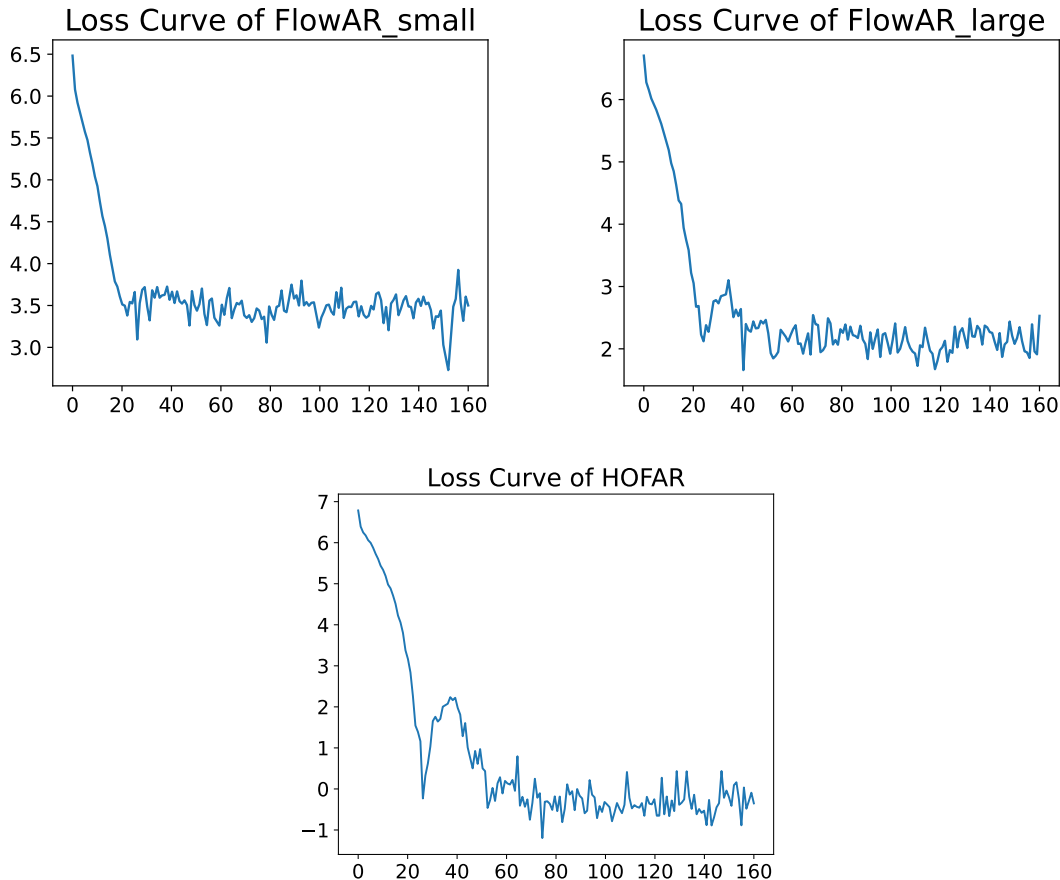
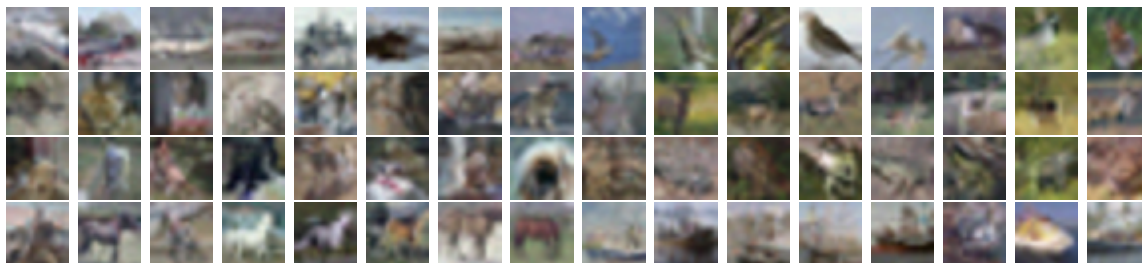


Figure 1: Loss curve of FlowAR-small (**Left**), loss curve of FlowAR-large (**Right**) and loss curve of HOFAR (**Bottom**).

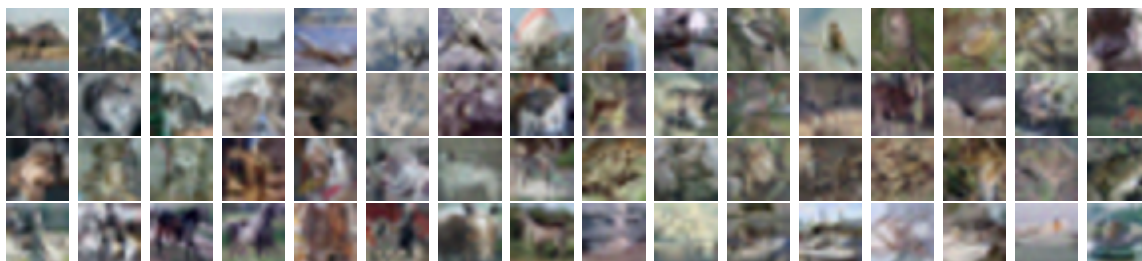
by the FlowAR-small, FlowAR-large and HOFAR, highlighting differences in color accuracy and generation quality on CIFAR-10 images.

### 6.1 Experiment Setup

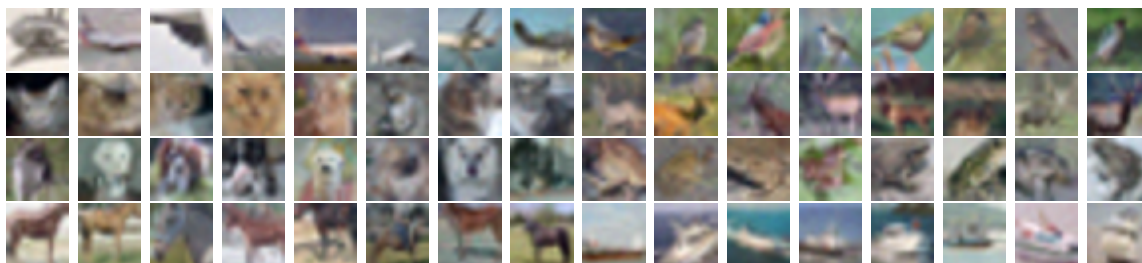
In FlowAR-small, we employ an embedding with three dimensions, and its Autoregressive component is configured with a 1024-dimensional feature space across a depth of 2 layers. Additionally, the flow-matching component is realized through a single hidden layer MLP operating with a step increment of 25. By comparison, FlowAR-large distinguishes itself by utilizing an eight dimension embedding and extending the Autoregressive feature dimension to 1536, while retaining the same configuration for the remaining components as in FlowAR-small. In the case of HOFAR, an embedding of dimension three is similarly adopted, paired with a 1024 dimension Autoregressive component structured over two layers, and a single-hidden-layer MLP is again employed for flow-matching with 25 steps. All three models were evaluated on the CIFAR-10 dataset, with analysis restricted to 8 classes due to computational constraints. All models above use AdamW optimizer with 0.0001 learning rate. In all experiments, the models were optimized by minimizing the sum of squared errors (SSE), and performance assessment during testing was based on the Euclidean distance metric. Regarding the target transport trajectory, we integrated the VP



(a) Images generated by FlowAR-small.



(b) Images generated by FlowAR-large.



(c) Images generated by HOFAR.

Figure 2: Comparison of 32\*32 CIFAR-10 images generation by FlowAR-small (**first four lines**), FlowAR-large (**second four lines**) and HOFAR (**last four lines**). For better looking, we put higher-resolution version of Figure 3, Figure 4 and Figure 5 here.

ODE framework as described in [LGL22], represented by  $x_t = \alpha_t x_0 + \beta_t x_1$ . Here,  $\alpha_t$  is defined as  $\exp(-\frac{1}{4}a(1-t)^2 - \frac{1}{2}b(1-t))$ , and  $\beta_t$  is determined by  $\sqrt{1 - \alpha_t^2}$ , with the hyperparameters fixed at  $a = 19.9$  and  $b = 0.1$ . During generation, the eight distinct training labels were provided as input, and a consistent *cfg* value of 4.3 was maintained for all three models.

## 6.2 Loss Function Curve

Now, we present the testing loss curves of the various models during training, providing insights into their convergence behavior and learning dynamics. Figure 1 illustrates the loss for FlowAR-small, FlowAR-large, and our HOFAR, with the respective model parameter counts being 170.70M, 222.72M, and 212.44M.

## 6.3 Visualization Comparison

As Figure 2 shows, the visualization instances generated by the FlowAR-small, FlowAR-large and HOFAR models are delineated in this study. Each model uses the same prompt at the corresponding position.

## 7 Conclusion

In this work, we presented High-Order FlowAR (HOFAR), a novel framework that integrates high-order dynamics into flow-matching-based auto-regressive generation. By modeling higher-order interactions, HOFAR enhances the ability to capture complex dependencies, leading to improved realism, coherence in generative tasks. Our theoretical analysis demonstrates that HOFAR maintains computational efficiency while benefiting from high-order. Empirical evaluations further validate the superiority of HOFAR over existing auto-regressive generative models. These contributions highlight the potential of incorporating high-order dynamics into generative frameworks, paving the way for more advanced generative models in the future.

## References

- [AAA<sup>+</sup>23] Josh Achiam, Steven Adler, Sandhini Agarwal, Lama Ahmad, Ilge Akkaya, Florencia Leoni Aleman, Diogo Almeida, Janko Altenschmidt, Sam Altman, Shyamal Anadkat, et al. Gpt-4 technical report. *arXiv preprint arXiv:2303.08774*, 2023.
- [CC82] George Corliss and YF Chang. Solving ordinary differential equations using taylor series. *ACM Transactions on Mathematical Software (TOMS)*, 8(2):114–144, 1982.
- [CC94] YF Chang and George Corliss. Atomft: solving odes and daes using taylor series. *Computers & Mathematics with Applications*, 28(10-12):209–233, 1994.
- [CCL<sup>+</sup>25] Yang Cao, Bo Chen, Xiaoyu Li, Yingyu Liang, Zhizhou Sha, Zhenmei Shi, Zhao Song, and Mingda Wan. Force matching with relativistic constraints: A physics-inspired approach to stable and efficient generative modeling. *arXiv preprint arXiv:2502.08150*, 2025.
- [CGL<sup>+</sup>25a] Yuefan Cao, Chengyue Gong, Xiaoyu Li, Yingyu Liang, Zhizhou Sha, Zhenmei Shi, and Zhao Song. Richspace: Enriching text-to-video prompt space via text embedding interpolation. *arXiv preprint arXiv:2501.09982*, 2025.
- [CGL<sup>+</sup>25b] Bo Chen, Chengyue Gong, Xiaoyu Li, Yingyu Liang, Zhizhou Sha, Zhenmei Shi, Zhao Song, Wan Mingda, and Xugang Ye. Nrflow: Towards noise-robust generative modeling via high-order mechanism. *Manuscript*, 2025.
- [CGL<sup>+</sup>25c] Bo Chen, Chengyue Gong, Xiaoyu Li, Yingyu Liang, Zhizhou Sha, Zhenmei Shi, Zhao Song, and Mingda Wan. High-order matching for one-step shortcut diffusion models. *arXiv preprint arXiv:2502.00688*, 2025.
- [CLL<sup>+</sup>25] Yuefan Cao, Xiaoyu Li, Yingyu Liang, Zhizhou Sha, Zhenmei Shi, Zhao Song, and Jiahao Zhang. Dissecting submission limit in desk-rejections: A mathematical analysis of fairness in ai conference policies. *arXiv preprint arXiv:2502.00690*, 2025.
- [CRBD18] Ricky TQ Chen, Yulia Rubanova, Jesse Bettencourt, and David K Duvenaud. Neural ordinary differential equations. *Advances in neural information processing systems*, 31, 2018.
- [Dee24] Google Deepmind. Gemini2, 2024.

- [DNG<sup>+</sup>22] Franck Djeumou, Cyrus Neary, Eric Goubault, Sylvie Putot, and Ufuk Topcu. Taylor-lagrange neural ordinary differential equations: Toward fast training and evaluation of neural odes. *arXiv:2201.05715*, 2022.
- [DY24] Yusuf Dalva and Pinar Yanardag. Noiseclr: A contrastive learning approach for unsupervised discovery of interpretable directions in diffusion models. In *Proceedings of the IEEE/CVF Conference on Computer Vision and Pattern Recognition*, pages 24209–24218, 2024.
- [EKB<sup>+</sup>24] Patrick Esser, Sumith Kulal, Andreas Blattmann, Rahim Entezari, Jonas Müller, Harry Saini, Yam Levi, Dominik Lorenz, Axel Sauer, Frederic Boesel, et al. Scaling rectified flow transformers for high-resolution image synthesis. In *Forty-first international conference on machine learning*, 2024.
- [FJNO20] Chris Finlay, Jörn-Henrik Jacobsen, Levon Nurbekyan, and Adam Oberman. How to train your neural ode: the world of jacobian and kinetic regularization. In *International conference on machine learning*, pages 3154–3164. PMLR, 2020.
- [GCB<sup>+</sup>18] Will Grathwohl, Ricky TQ Chen, Jesse Bettencourt, Ilya Sutskever, and David Duvenaud. Ffjord: Free-form continuous dynamics for scalable reversible generative models. *arXiv preprint arXiv:1810.01367*, 2018.
- [GKL<sup>+</sup>25] Chengyue Gong, Yekun Ke, Xiaoyu Li, Yingyu Liang, Zhizhou Sha, Zhenmei Shi, and Zhao Song. On computational limits of flowar models: Expressivity and efficiency. *arXiv preprint arXiv:2502.16490*, 2025.
- [GXX<sup>+</sup>24] Yuming Gu, Hongyi Xu, You Xie, Guoxian Song, Yichun Shi, Di Chang, Jing Yang, and Linjie Luo. Diffportrait3d: Controllable diffusion for zero-shot portrait view synthesis. In *Proceedings of the IEEE/CVF Conference on Computer Vision and Pattern Recognition*, pages 10456–10465, 2024.
- [GYZ<sup>+</sup>25] Daya Guo, Dejian Yang, Haowei Zhang, Junxiao Song, Ruoyu Zhang, Runxin Xu, Qihao Zhu, Shirong Ma, Peiyi Wang, Xiao Bi, et al. Deepseek-r1: Incentivizing reasoning capability in llms via reinforcement learning. *arXiv preprint arXiv:2501.12948*, 2025.
- [HHS23] Emiel Hoogeboom, Jonathan Heek, and Tim Salimans. simple diffusion: End-to-end diffusion for high resolution images. In *International Conference on Machine Learning*, pages 13213–13232. PMLR, 2023.
- [HJA20] Jonathan Ho, Ajay Jain, and Pieter Abbeel. Denoising diffusion probabilistic models. *Advances in neural information processing systems*, 33:6840–6851, 2020.
- [HLJ<sup>+</sup>24] Seongmin Hong, Kyeonghyun Lee, Suh Yoon Jeon, Hyewon Bae, and Se Young Chun. On exact inversion of dpm-solvers. In *Proceedings of the IEEE/CVF Conference on Computer Vision and Pattern Recognition*, pages 7069–7078, 2024.
- [HST<sup>+</sup>22] Hang Hu, Zhao Song, Runzhou Tao, Zhaozhuo Xu, Junze Yin, and Danyang Zhuo. Sublinear time algorithm for online weighted bipartite matching. *arXiv preprint arXiv:2208.03367*, 2022.

- [HSZ<sup>+</sup>24] Xin Huang, Ruizhi Shao, Qi Zhang, Hongwen Zhang, Ying Feng, Yebin Liu, and Qing Wang. Humannorm: Learning normal diffusion model for high-quality and realistic 3d human generation. In *Proceedings of the IEEE/CVF Conference on Computer Vision and Pattern Recognition*, pages 4568–4577, 2024.
- [HWL<sup>+</sup>25] Jerry Yao-Chieh Hu, Weimin Wu, Yi-Chen Lee, Yu-Chao Huang, Minshuo Chen, and Han Liu. On statistical rates of conditional diffusion transformers: Approximation, estimation and minimax optimality. In *The Thirteenth International Conference on Learning Representations*, 2025.
- [HZY<sup>+</sup>25] Mude Hui, Rui-Jie Zhu, Songlin Yang, Yu Zhang, Zirui Wang, Yuyin Zhou, Jason Eshraghian, and Cihang Xie. Arflow: Autogressive flow with hybrid linear attention. *arXiv preprint arXiv:2501.16085*, 2025.
- [JSL<sup>+</sup>24] Yang Jin, Zhicheng Sun, Ningyuan Li, Kun Xu, Hao Jiang, Nan Zhuang, Quzhe Huang, Yang Song, Yadong Mu, and Zhouchen Lin. Pyramidal flow matching for efficient video generative modeling. *arXiv preprint arXiv:2410.05954*, 2024.
- [JWT<sup>+</sup>24] Siddhant Jain, Daniel Watson, Eric Tabellion, Ben Poole, Janne Kontkanen, et al. Video interpolation with diffusion models. In *Proceedings of the IEEE/CVF Conference on Computer Vision and Pattern Recognition*, pages 7341–7351, 2024.
- [KBJD20] Jacob Kelly, Jesse Bettencourt, Matthew J Johnson, and David K Duvenaud. Learning differential equations that are easy to solve. *Advances in Neural Information Processing Systems*, 33:4370–4380, 2020.
- [KLL<sup>+</sup>25] Yekun Ke, Xiaoyu Li, Yingyu Liang, Zhizhou Sha, Zhenmei Shi, and Zhao Song. On computational limits and provably efficient criteria of visual autoregressive models: A fine-grained complexity analysis. *arXiv preprint arXiv:2501.04377*, 2025.
- [KLS<sup>+</sup>25] Yekun Ke, Yingyu Liang, Zhizhou Sha, Zhenmei Shi, and Zhao Song. Dpbloomfilter: Securing bloom filters with differential privacy. *arXiv preprint arXiv:2502.00693*, 2025.
- [LCBH<sup>+</sup>22] Yaron Lipman, Ricky TQ Chen, Heli Ben-Hamu, Maximilian Nickel, and Matt Le. Flow matching for generative modeling. *arXiv preprint arXiv:2210.02747*, 2022.
- [LCW<sup>+</sup>23] Xin Li, Wenqing Chu, Ye Wu, Weihang Yuan, Fanglong Liu, Qi Zhang, Fu Li, Haocheng Feng, Errui Ding, and Jingdong Wang. Videogen: A reference-guided latent diffusion approach for high definition text-to-video generation. *arXiv preprint arXiv:2309.00398*, 2023.
- [LGL22] Xingchao Liu, Chengyue Gong, and Qiang Liu. Flow straight and fast: Learning to generate and transfer data with rectified flow. *arXiv preprint arXiv:2209.03003*, 2022.
- [LLSS24] Chenyang Li, Yingyu Liang, Zhenmei Shi, and Zhao Song. Exploring the frontiers of softmax: Provable optimization, applications in diffusion model, and beyond. *arXiv preprint arXiv:2405.03251*, 2024.
- [LSS<sup>+</sup>24] Yingyu Liang, Zhizhou Sha, Zhenmei Shi, Zhao Song, and Yufa Zhou. Multi-layer transformers gradient can be approximated in almost linear time. *arXiv preprint arXiv:2408.13233*, 2024.

- [LSS<sup>+</sup>25] Yingyu Liang, Zhizhou Sha, Zhenmei Shi, Zhao Song, Wan Mingda, and Yufa Zhou. Unraveling the smoothness properties of diffusion models: A gaussian mixture perspective. *Manuscript*, 2025.
- [LSSS24] Yingyu Liang, Zhizhou Sha, Zhenmei Shi, and Zhao Song. Differential privacy mechanisms in neural tangent kernel regression. *arXiv preprint arXiv:2407.13621*, 2024.
- [LTL<sup>+</sup>24] Tianhong Li, Yonglong Tian, He Li, Mingyang Deng, and Kaiming He. Autoregressive image generation without vector quantization. *arXiv preprint arXiv:2406.11838*, 2024.
- [LYX<sup>+</sup>24] Hanwen Liang, Yuyang Yin, Dejie Xu, Hanxue Liang, Zhangyang Wang, Konstantinos N Plataniotis, Yao Zhao, and Yunchao Wei. Diffusion4d: Fast spatial-temporal consistent 4d generation via video diffusion models. *arXiv preprint arXiv:2405.16645*, 2024.
- [LZW<sup>+</sup>24] Chengyi Liu, Jiahao Zhang, Shijie Wang, Wenqi Fan, and Qing Li. Score-based generative diffusion models for social recommendations. *arXiv preprint arXiv:2412.15579*, 2024.
- [Mo24] Shentong Mo. Efficient 3d shape generation via diffusion mamba with bidirectional ssms. *arXiv preprint arXiv:2406.05038*, 2024.
- [RBL<sup>+</sup>22] Robin Rombach, Andreas Blattmann, Dominik Lorenz, Patrick Esser, and Björn Ommer. High-resolution image synthesis with latent diffusion models. In *Proceedings of the IEEE/CVF conference on computer vision and pattern recognition*, pages 10684–10695, 2022.
- [RCK<sup>+</sup>24] Litu Rout, Yujia Chen, Abhishek Kumar, Constantine Caramanis, Sanjay Shakkottai, and Wen-Sheng Chu. Beyond first-order tweedie: Solving inverse problems using latent diffusion. In *Proceedings of the IEEE/CVF Conference on Computer Vision and Pattern Recognition*, pages 9472–9481, 2024.
- [RYH<sup>+</sup>24] Sucheng Ren, Qihang Yu, Ju He, Xiaohui Shen, Alan Yuille, and Liang-Chieh Chen. Flowar: Scale-wise autoregressive image generation meets flow matching. *arXiv preprint arXiv:2412.15205*, 2024.
- [SPH<sup>+</sup>22] Uriel Singer, Adam Polyak, Thomas Hayes, Xi Yin, Jie An, Songyang Zhang, Qiyuan Hu, Harry Yang, Oron Ashual, Oran Gafni, et al. Make-a-video: Text-to-video generation without text-video data. *arXiv preprint arXiv:2209.14792*, 2022.
- [SSZ<sup>+</sup>24] Xuan Shen, Zhao Song, Yufa Zhou, Bo Chen, Yanyu Li, Yifan Gong, Kai Zhang, Hao Tan, Jason Kuen, Henghui Ding, et al. Lazydit: Lazy learning for the acceleration of diffusion transformers. *arXiv preprint arXiv:2412.12444*, 2024.
- [SWYY25] Zhao Song, Weixin Wang, Chenbo Yin, and Junze Yin. Fast and efficient matching algorithm with deadline instances. In *The Second Conference on Parsimony and Learning (Proceedings Track)*, 2025.
- [TJY<sup>+</sup>25] Keyu Tian, Yi Jiang, Zehuan Yuan, Bingyue Peng, and Liwei Wang. Visual autoregressive modeling: Scalable image generation via next-scale prediction. *Advances in neural information processing systems*, 37:84839–84865, 2025.

- [WCZ<sup>+</sup>23] Yilin Wang, Zeyuan Chen, Liangjun Zhong, Zheng Ding, Zhizhou Sha, and Zhuowen Tu. Dolfn: Diffusion layout transformers without autoencoder. *arXiv preprint arXiv:2310.16305*, 2023.
- [WFQ<sup>+</sup>24] Wei Wu, Qingnan Fan, Shuai Qin, Hong Gu, Ruoyu Zhao, and Antoni B Chan. Freediff: Progressive frequency truncation for image editing with diffusion models. In *European Conference on Computer Vision*, pages 194–209. Springer, 2024.
- [WSD<sup>+</sup>24] Zirui Wang, Zhizhou Sha, Zheng Ding, Yilin Wang, and Zhuowen Tu. Tokencompose: Text-to-image diffusion with token-level supervision. In *Proceedings of the IEEE/CVF Conference on Computer Vision and Pattern Recognition*, pages 8553–8564, 2024.
- [WXZ<sup>+</sup>24] Yilin Wang, Haiyang Xu, Xiang Zhang, Zeyuan Chen, Zhizhou Sha, Zirui Wang, and Zhuowen Tu. Omnicontrolnet: Dual-stage integration for conditional image generation. In *Proceedings of the IEEE/CVF Conference on Computer Vision and Pattern Recognition*, pages 7436–7448, 2024.
- [XXMPM24] Yuxuan Xue, Xianghui Xie, Riccardo Marin, and Gerard Pons-Moll. Gen-3diffusion: Realistic image-to-3d generation via 2d & 3d diffusion synergy. *arXiv preprint arXiv:2412.06698*, 2024.
- [XZL<sup>+</sup>24] Zhongcong Xu, Jianfeng Zhang, Jun Hao Liew, Hanshu Yan, Jia-Wei Liu, Chenxu Zhang, Jiashi Feng, and Mike Zheng Shou. Magicanimate: Temporally consistent human image animation using diffusion model. In *Proceedings of the IEEE/CVF Conference on Computer Vision and Pattern Recognition*, pages 1481–1490, 2024.
- [ZCW<sup>+</sup>25] Haiyu Zhang, Xinyuan Chen, Yaohui Wang, Xihui Liu, Yunhong Wang, and Yu Qiao. 4diffusion: Multi-view video diffusion model for 4d generation. *Advances in Neural Information Processing Systems*, 37:15272–15295, 2025.

# Appendix

**Roadmap.** In Section A, we analyze the strengths and limitations of the High-Order FlowAR (HOFAR) framework. In Section B, we exhibit some result obtained from the experiments.

## A Discussion

The HOFAR framework introduces a novel approach to integrating high-order dynamics into flow-matching-based auto-regressive generation, significantly improving the modeling of complex dependencies and generation quality. However, certain limitations and future directions deserve attention. One limitation is the potential computational overhead when scaling HOFAR to extremely high-dimensional data, such as ultra-high-resolution images or long-duration videos. While HOFAR maintains theoretical efficiency, practical implementation may require further optimization to handle such scenarios. Future work could explore extending HOFAR to multi-modal generation tasks, such as joint text-video or text-3D generation, where capturing long-term coherence across modalities is critical. Furthermore, improving the interpretability of high-order dynamics through visualization or disentanglement techniques would broaden HOFAR’s applicability.

## B Empirical Result

In Section B.1, we compare visualizations generated by FlowAR and our HOFAR, this highlighting differences in color accuracy and relative position on CIFAR-10 images.

### B.1 Visualization Examples

We present visualization examples produced by the FlowAR-small, FlowAR-large and proposed HOFAR. Specifically, Figure 3 showcases visualizations generated by the FlowAR-small model, Figure 4 showcases visualizations generated by the FlowAR-large model, whereas Figure 5 highlights visualizations created by the HOFAR model.

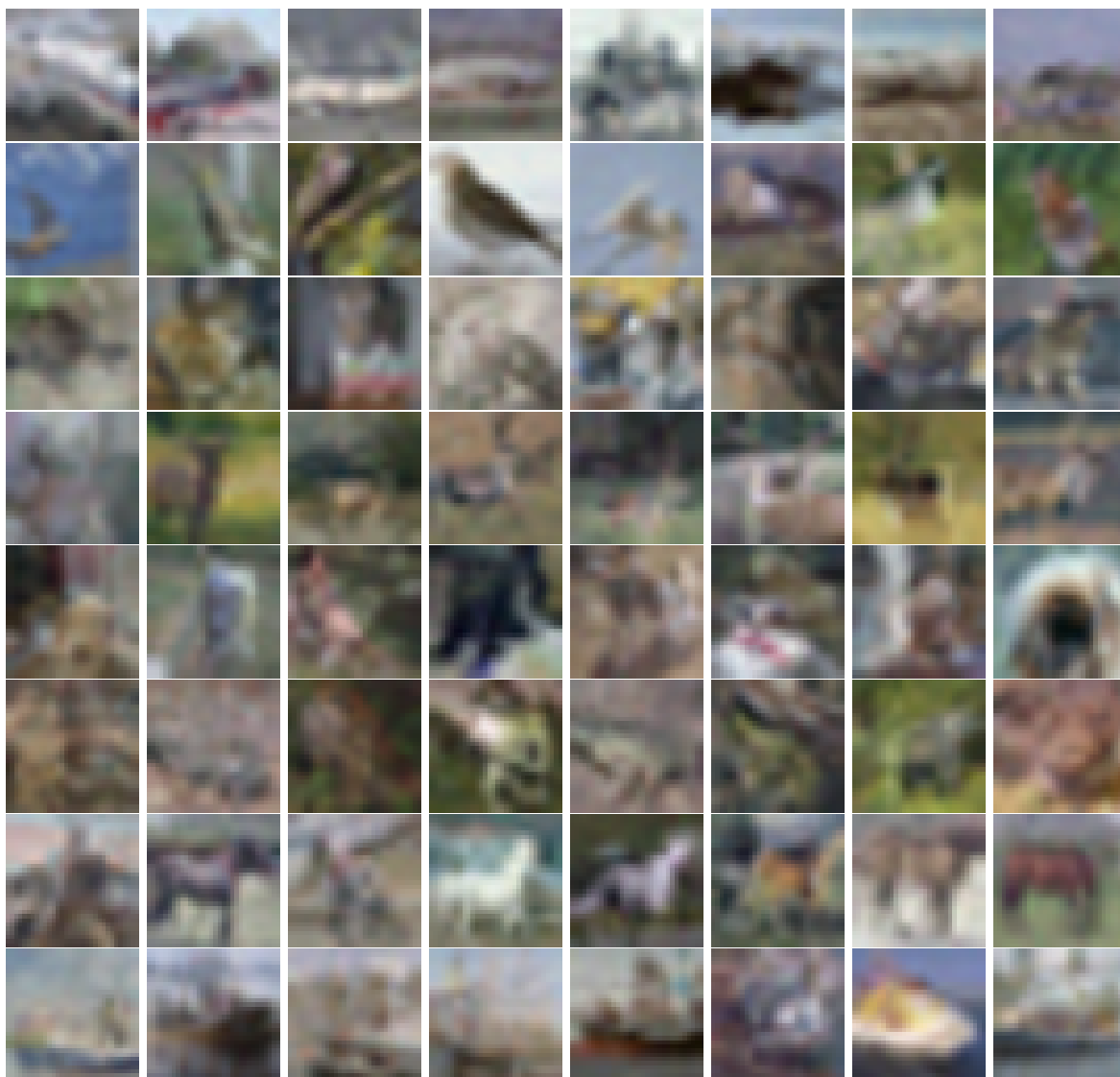


Figure 3: 64 32\*32 images generated by FlowAR-small.

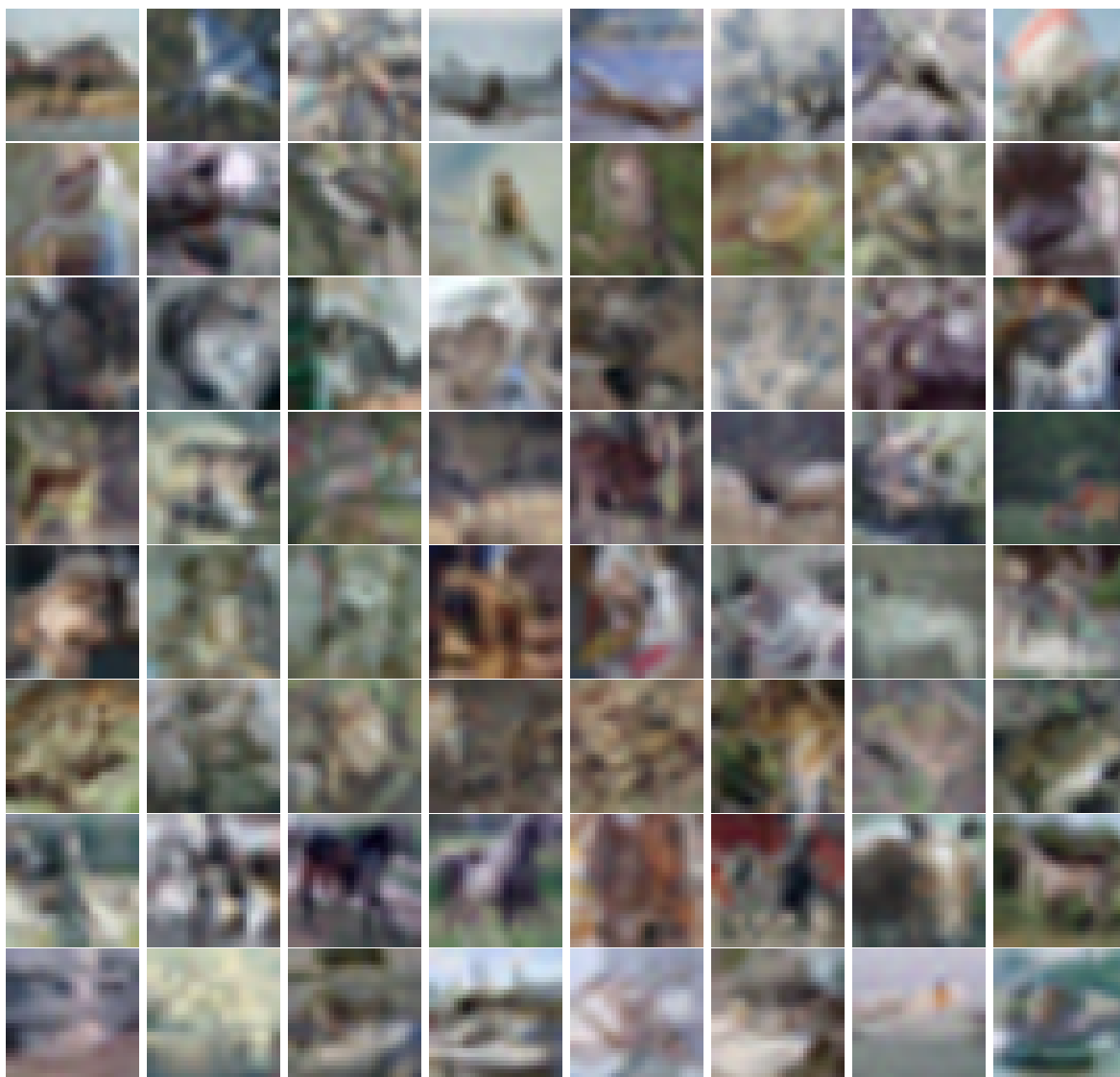


Figure 4: 64 32\*32 images generated by FlowAR-large.

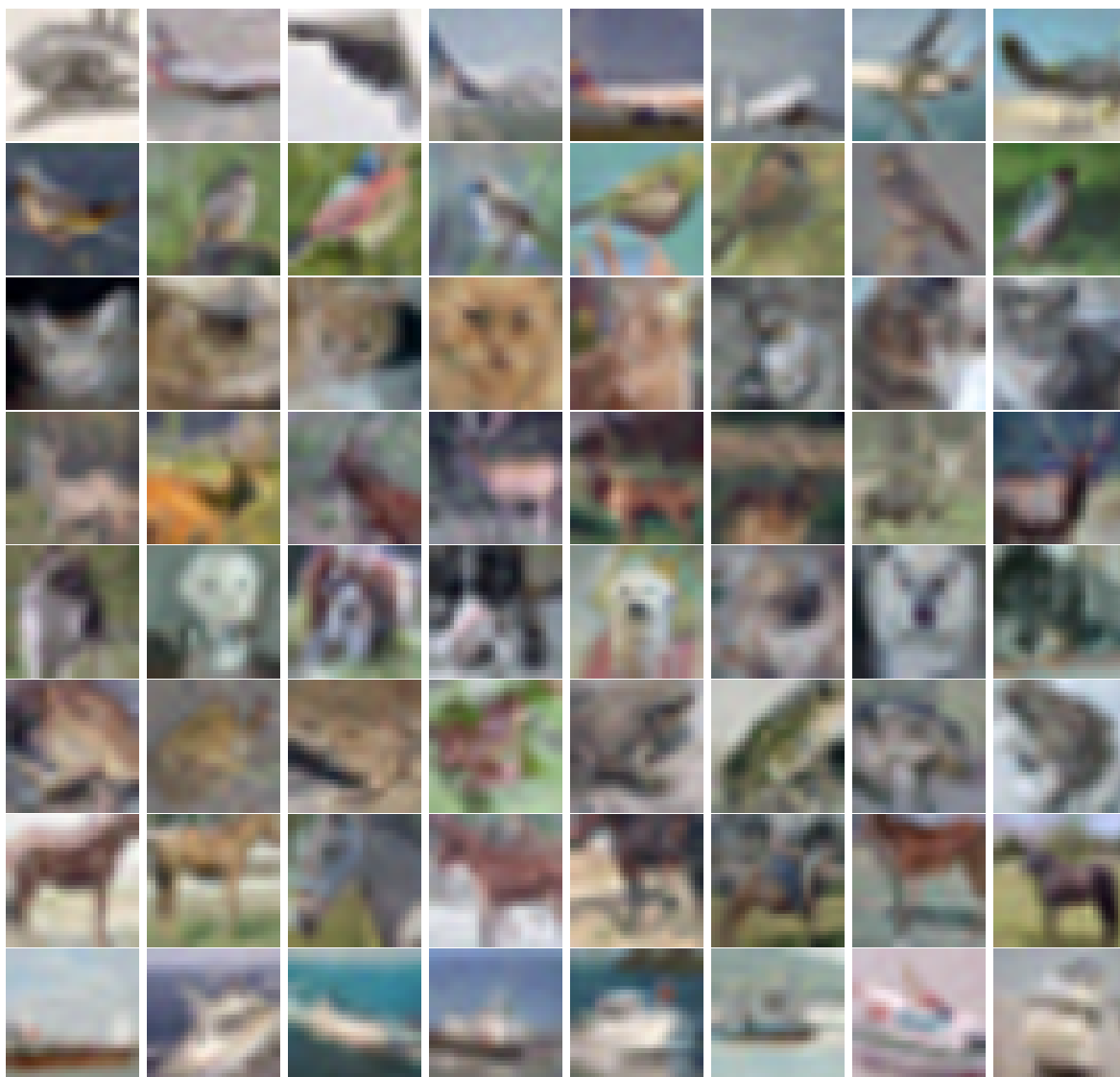


Figure 5: 64 32\*32 images generated by HOFAR.